molecular pharmaceutics

pubs.acs.org/molecularpharmaceutics

Article

New Insights into the Crystallographic Disorder in the Polymorphic Forms of Aspirin from Low-Frequency Vibrational Analysis

Qi Li, Andrew D. Bond, Timothy M. Korter, and J. Axel Zeitler*

Cite This: *Mol. Pharmaceutics* 2022, 19, 227−234

Read Online

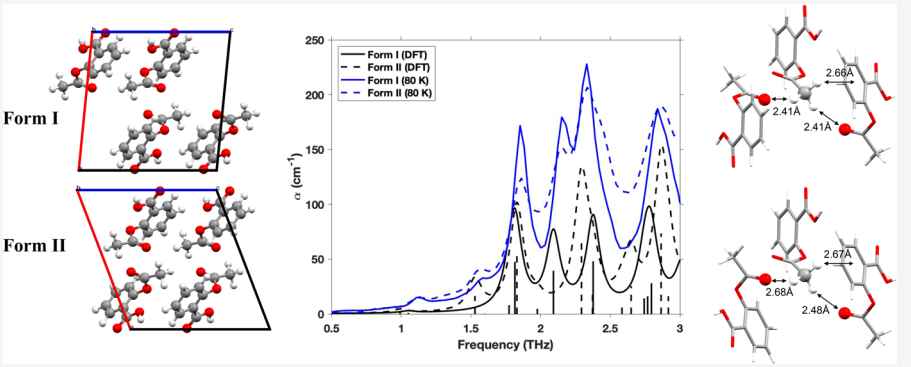

ABSTRACT: Terahertz time-domain spectroscopy (THz-TDS) is applied to two polymorphs of acetylsalicylic acid (aspirin), and the experimental spectra are compared to lattice dynamical calculations using high accuracy density functional theory. The calculations confirm that forms I and II have very close energetic and thermodynamic properties and also that they show similar spectral features in the far-infrared region, reflecting the high degree of similarity in their crystal structures. Unique vibrational modes are identified for each polymorph which allow them to be distinguished using THz-TDS measurements. The observation of spectral features attributable to both polymorphic forms in a single sample, however, provides further evidence to support the hypothesis that crystalline aspirin typically comprises intergrown domains of forms I and II. Differences observed in the baseline of the measured THz-TDS spectra indicate a greater degree of structural disorder in the samples of form II. Calculated Gibbs free-energy curves show a turning point at 75 K, inferring that form II is expected to be more stable than form I above this temperature as a result of its greater vibrational entropy. The calculations do not account for any differences in configurational entropy that may arise from expected structural defects. Further computational work on these structures, such as ab initio molecular dynamics, would be very useful to further explore this perspective. Here, aspirin is a model system to show how the additional insight from the low-frequency vibrational information complements the structural data and allows for quantitative thermodynamic information of pharmaceutical polymorphs to be extracted. The methodology is directly applicable to other polymorphic systems.

KEYWORDS: *aspirin, polymorphism, THz-TDS, DFT simulations, XRPD*

1. INTRODUCTION

The crystal structure of one of the most well-known analgesics, acetylsalicylic acid, commonly referred to under its trade name aspirin, was first characterized by Wheatley in 1964.[1] After the initial crystal structure was determined, it was widely discussed whether other crystal forms of aspirin may exist, but it was not until 2005 that Vishweshwar et al. reported the crystal structure of aspirin form II.[2] The form II structure had been identified as an energy minimum by Ouvrard and Price[3] in a crystal structure prediction exercise, but suboptimal features of the experimental structure determination left doubts over the validity of the crystal structure and the existence of form II as a discrete polymorph.[4] The origin of these difficulties was explained by Bond et al., who showed that aspirin forms I and II exist as intergrown single crystals, comprising domains of both structure types.[5] Reproducible crystallization of form II remained challenging, but it was shown in 2010 that domains of the second polymorph of aspirin are introduced reliably in the presence of aspirin anhydride during the crystallization process.[6] More polymorphs of aspirin have since been discovered. A high-pressure polymorph form III has been observed from changes in Raman spectra on compression of form I above 2 GPa.[7] A further polymorph (form IV) obtained

Received: September 17, 2021
Revised: November 18, 2021
Accepted: November 18, 2021
Published: December 2, 2021

from the melt has been structurally characterized at ambient conditions, but it transforms to form I within a couple of minutes at room temperature.[8] Given their limited stability, these additional forms are not considered in this study.

In this paper, we focus on the closely related aspirin polymorphs, form I and form II. There are considerable similarities in their respective crystal structures, which permit the observed intergrowth behavior. Figure 1 shows the

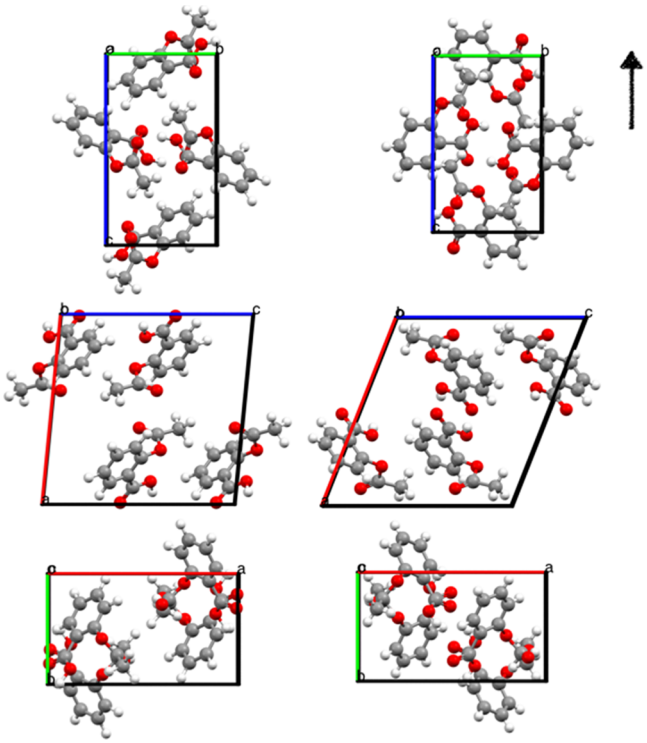

Figure 1. Projections of aspirin form I (left) and form II (right) viewed from *a*, *b*, and *c* axes (from top to bottom). The arrow next to the *a*-axis points in the direction of the *c*-axis. It emphasizes the relationship between the two polymorphs by shifting neighboring layers by half a unit-cell length in this direction.

projections of the two polymorphs along the *a*, *b*, and *c* axes. The structures are polytypes[9] having consistent layers lying in the *bc* planes. For the two forms, the difference is seen in the arrangement of these layers along the *a*-axis. The relationship between the structures can be viewed as a shift of neighboring layers by half a unit-cell length along the *c*-axis (as can be seen in the *a* axis projection) or alternatively as a reflection of every second layer perpendicular to the *b*-axis. Given the observed intergrowth behavior, it is evident that the two arrangements must have closely comparable energies. Computational work using density functional theory (DFT) has indicated that the two forms exhibit only a subtle energetic difference, and it was suggested that the two polymorphs were virtually degenerate.[10] Later on, Reilly and Tkatchenko applied a many-body dispersion approach with DFT to investigate their energetic differences at room temperature, which inferred that the stability of form I was due to the coupling of low-frequency phonon modes and collective electronic fluctuations.[11] A recent work of Vaksler et al. proposed a new method to study the mechanical properties using quantum chemical calculations constituted of two steps: analysis of the pairwise interactions between molecules and modeling displacement between strongly bound fragments.[12] The results identified the crystallographic *c*-axis, within the region between the common planes of the polytypes, as the most likely direction for shear deformation to occur.

Even though crystals are defined as well-organized and ordered systems, defects and dislocations are commonly encountered in crystalline materials. The influence of defects, for example, on the properties of metals, has been widely studied. It is well known that defects can also affect the performance of molecular materials such as their mechanical stability.[13] The subtle differences in the crystal structure between the two aspirin forms and the comparable energetic stabilities challenge the view of distinct polymorphs and make this an interesting model system for investigating the effect of disorder and the structural dynamics in organic molecular crystals beyond their perfect structures. Chan et al. have reported a detailed structural study of aspirin crystals, with disorder models fitted to diffuse X-ray scattering data.[14] These results confirm that crystals of form I are well ordered but that form II crystals contain stacking faults corresponding to the form I interlayer arrangement, which aggregate to produce included regions of the form I structure. Hence, "pure" form II is generally not encountered and may not be experimentally attainable.

Well-established solid-state analytical techniques can probe a wide range of molecular, particulate, and bulk properties. For example, by combining information from spectroscopic techniques (i.e., Raman and Fourier transform infrared spectroscopies), X-ray diffraction, differential scanning calorimetry, as well as thermogravimetric analysis,[15] a thorough characterization of the sample of interest can be achieved. The method proposed in this study augments this approach by combining vibrational spectroscopy in the far-infrared region, measured by terahertz time-domain spectroscopy (THz-TDS), and ab initio DFT simulations under periodic boundary conditions. The unique perspective this adds is to explicitly take into account the influence of low-frequency vibrational dynamics. These motions typically exhibit a large amplitude and are very soft and complex motions dictated by the weak dispersion and hydrogen-bonding interactions in organic molecular crystals. We show here how this information can reveal further insight regarding the nature of polymorphism in the examples of aspirin forms I and II. These low-frequency dynamics are of universal importance for crystal polymorphism, and the approach described in this work can be applied directly to many other pharmaceutical systems of interest. The measurement of vibrational dynamics complements the structural characterization from crystallographic techniques, while the solid-state DFT methods provide a powerful route for interpretation of the THz spectra. These methodologies have previously been applied to study a wide range of organic molecular crystals, including polymorphs of pharmaceutical drug molecules.[16−19] THz-TDS probes weak interactions within molecular crystals, but due to the complexity of the motions at THz frequencies, not least given the strong coupling between large amplitude external and internal motions, the spectra are difficult to interpret without the complementary DFT method. The THz spectrum of aspirin form I has previously been measured by Laman, Harsha, and Grischkowsky using a bespoke THz-TDS setup, where thin films of crystals were grown directly onto the surface of an aluminum parallel plate waveguide structure.[20] This method has the advantage that no scattering occurs when

https://doi.org/10.1021/acs.molpharmaceut.1c00727
Mol. Pharmaceutics 2022, 19, 227−234

the THz electric field propagates along the surface of the waveguide and the effervescent field can interact very efficiently with the crystalline film. As a result, the line width of the vibrational modes is dramatically sharpened compared to conventional transmission spectroscopy of a polycrystalline sample (Figure S1). However, the requirement to crystallize the sample directly onto the flat aluminum plate waveguides in the form of a thin film restricts the application of the method for a detailed investigation of complex polymorphism, where such constraints in crystallization conditions limit the accessible solid-state forms. Therefore, we apply transmission measurements on pellets containing polycrystalline particles of the two polymorphic forms of aspirin using a commercial THz spectrometer.

2. EXPERIMENTAL SECTION

2.1. Materials. Commercial aspirin form I of USP grade was acquired from Sigma-Aldrich (Gillingham, UK) and used as received. Form II was prepared following the procedure described by Bond et al. through crystallization from the organic solution of form I in the presence of aspirin anhydride.[6] A bulk solid mixture of 9 g of aspirin and 1 g of aspirin anhydride was prepared and divided into 10 × 1 g portions in separate vials. The solid in each vial was dissolved in 3 mL of tetrahydrofuran with shaking and then left to evaporate under ambient conditions. X-ray powder diffraction (XRPD) was used to confirm the crystalline structure of all samples prior to any subsequent THz spectroscopy experiments.

2.2. XRPD. XRPD measurements were carried out on a Panalytical XPert Pro diffractometer in Bragg−Brentano geometry using non-monochromated Cu Kα radiation (λ_{ave} = 1.5418 Å). Samples were prepared on glass flat-plate sample holders, and data were measured over the range 2θ = 3−40 °. Due to the polytypic relationship between the crystal structures, the diffraction patterns of aspirin form I and II are closely comparable (50% of the reflections are identical). Form II domains are indicated by signature peaks at $2\theta \approx$ 16.0, 19.2, and 26.0°.[5]

2.3. THz-TDS. The THz-TDS measurements were performed in transmission using a commercial spectrometer (TeraPulse 4000, TeraView Ltd., Cambridge, UK) equipped with a cryostat (Janis, Massachusetts, USA) and an attached temperature controller (Lakeshore 330, Ohio, USA). The setup was used to acquire measurements in the temperature range between 80 and 400 K.

Due to the strong absorption from pure crystals, polycrystalline aspirin powder was diluted in polyethylene (PE) powder (Induchem, Volketwil, Switzerland) to a 5% w/w concentration using an agate mortar and pestle by gentle mixing. The powder mixture was then compressed into a pellet of 13 mm diameter using a hydraulic press (Specac Ltd., Kent, UK) with a load of 2 tons, and a blank PE pellet was prepared in the same way to be used as the reference. For each sample, 1000 waveforms were acquired and averaged with a spectral resolution of 0.94 cm^{-1}. A spectrum was first acquired at room temperature to check if the sample pellet was at the proper concentration. The whole system was then cooled to 80 K with liquid nitrogen to acquire a spectrum at low temperature that would be more comparable with the simulated spectrum from the DFT calculations.

2.4. DFT Calculations. The DFT simulations were performed using the CRYSTAL17 software package.[21] The published crystallographic data from the Cambridge Structural Database (ACSALA07; ACSALA17) were used to set the initial atomic positions and lattice parameters.[14,22,23] The subtle differences between the two polymorphs required very strict parameters for the best differentiation. The "extra extra large" grid (XXLGRID) was used to generate 100 *k*-points in the reciprocal space (SHRINK = 7), and the tolerances of bielectronic Coulomb and Hartree−Fock exchange integrals were set to 10^{-12}, 10^{-12}, 10^{-12}, 10^{-12}, and 10^{-24} (TOLINTEG). The atomic centered triple-ξ Ahlrichs' VTZ basis set (with polarization)[24] and the Perdew−Burke−Ernzerhof density functional[25] with Grimme-D3 London dispersion correction[26,27] were applied with a three-body Axilrod−Teller−Muto repulsion term (ABC).[28] The energy convergence criterion for the geometry optimization was set at 10^{-8} Hartree and 10^{-10} Hartree for the frequency analysis. The default DIIS convergence accelerator was applied. In addition, two displacements for each atom along each Cartesian direction were calculated for the phonon modes (NUMDERIV = 2), and the IR intensities were calculated based on the Berry phase method.[29,30] The cohesive energies of both forms were calculated by subtracting the isolated molecular energy from the total solid-state energy considering the basis set superposition error (BSSE), which originates from the finite basis sets.[31] Select normal modes were chosen, and the corresponding geometries were scanned along the eigenvectors to obtain more information on these modes (SCANMODE). The Gibbs free energy as well as other thermodynamic properties were calculated from 7 to 300 K for each structure.

3. RESULTS AND DISCUSSION

3.1. XRPD. The bulk solids from the crystallization trials contained differing degrees of form II domains, as indicated by the relative intensities of the signature form II peaks in the XRPD patterns (Figure S2). Trace aspirin anhydride was also detected in most samples. The variability in the crystallization outcome is attributed principally to (deliberate) inhomogenous mixing of the initial aspirin/aspirin anhydride solid sample. Three samples were selected for further analysis, which contained minimum quantities of aspirin anhydride and a range of form II peak intensities. The sample referred to as "form I" shows no evidence of form II peaks in the XRPD, "low purity form II" shows form II peaks of intermediate intensity, and "high purity form II" shows the most intense form II peaks (Figure 2). Here, "purity" refers to the polymorphic composition. Hence, the form I sample straightforwardly represents the aspirin form I structure, the high purity form II sample is the best available representative of the form II structure, and the low purity form II sample comprises the form II structure with a more substantial fraction of form I domains.

3.2. THz-TDS. The maximum absorption coefficient (α_{max}) was determined by the dynamic range of the THz signal.[32] It was checked qualitatively for the experimental results to make sure that the absorption was within the accessible range. Figure S3 shows that the absorption did not exceed the dynamic range of the instrument for frequencies up to 3 THz. Therefore, the spectra obtained for the two polymorphs were valid for further analysis.

Figure 3 shows the experimental spectra of form I and the two form II samples at 80 K. The overall resemblance of all parts of the spectra reflects the close structural similarity between the two forms, which is not generally common in

https://doi.org/10.1021/acs.molpharmaceut.1c00727
Mol. Pharmaceutics 2022, 19, 227−234

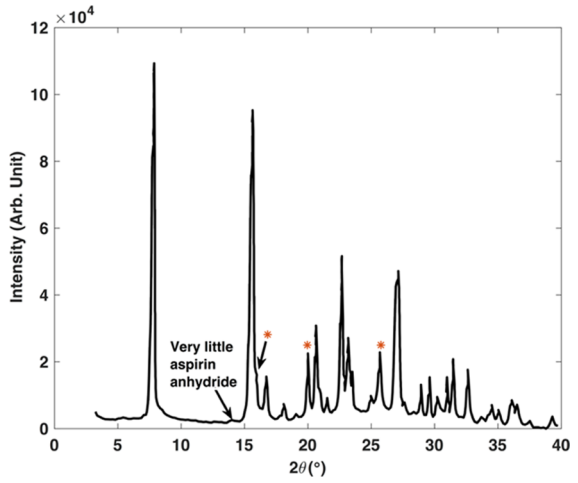

Figure 2. XRPD pattern of the high purity form II. The red asterisks highlight the characteristic peaks of form II that are absent in the diffraction pattern of form I.

other polymorphic systems. In order to facilitate comparison, the spectra were normalized relative to the peak at 1.8 THz, which is a pronounced feature in both forms (Figure 3). The reason for choosing this feature will be explained in the following section of computational results. In general, the peaks of form II appeared relatively broader than those of form I, which may reflect the inherent disorder expected for form II. The three main differences are pointed out in Figure 3: (i) the feature at around 1.5 THz is considerably more intense in the form II samples than in form I; (ii) around 2.0 THz, the spectra of the form II samples clearly show peak broadening and merging; (iii) the form II samples show a shoulder on the high-frequency flank of the peak just before 2.5 THz.

3.3. Optimization of the Crystal Structures. The experimental crystal structures of both polymorphic forms were optimized using the settings described in the Experimental section and compared with their published experimental data at 100 and 300 K (as shown in Tables S1 and S2). The relative errors between the experimental and optimized structures are small, demonstrating the accuracy of the calculations. As expected, the calculated physical properties of the two polymorphs (Table 1) show only marginal differences. The total lattice energy of form II is calculated

Table 1. Comparison of the Properties of the Two Polymorphs (Form I and Form II)[a]

	form I	form II	difference
energy (× 10^6 kJ mol^{-1})	−6.80803637	−6.80803608	−0.293
volume (Å^3)	834.803	832.476	2.328
density (g cm^{-3})	1.433	1.437	−0.004
$E_{cohesive}$ (kJ mol^{-1})	205.092	205.652	−0.560
$E_{cohesive}$ with BSSE (kJ mol^{-1})	10.285	10.250	0.035
zero-point energy (kJ mol^{-1})	1617.261	1615.945	1.316
entropy (J mol^{-1} K^{-1})	862.097	875.594	−13.497
heat capacity (J mol^{-1} K^{-1})	785.492	785.638	−0.146

[a]The entropy and heat capacity listed in the table are values predicted at 298.15 K and atmospheric pressure.

to be 0.293 kJ mol^{-1} higher than that of form I, which implies that form I is marginally the more energetically stable state. The energy difference increases to 1.609 kJ mol^{-1} when considering also the zero-point energies. The cohesive energy ($E_{cohesive}$ per molecule) of form I is predicted to be 0.560 kJ mol^{-1} lower than form II prior to any correction for BSSE but rises to 0.035 kJ mol^{-1} higher than form II after BSSE correction. A noticeable difference is that the entropy of form I is predicted to be smaller than that of form II. It should be noted that this refers to vibrational entropy, calculated for the idealized form I and form II crystal structures. The calculations do not quantify configurational entropy associated with the structural disorder described for form II single crystals.

3.4. Frequency Analysis. The simulated vibrational spectra were calculated for the optimized crystal structures and compared with the experimental results in Figure 4 (the experimental results of the high purity form II are used henceforth for further analysis). Figure 5 shows the simulated spectra of both forms with the bandwidth set to 1 cm^{-1} in order to display each feature for a clearer comparison. As shown, the peak at around 1.8 THz is predicted for both forms with comparable intensities and hence the decision to

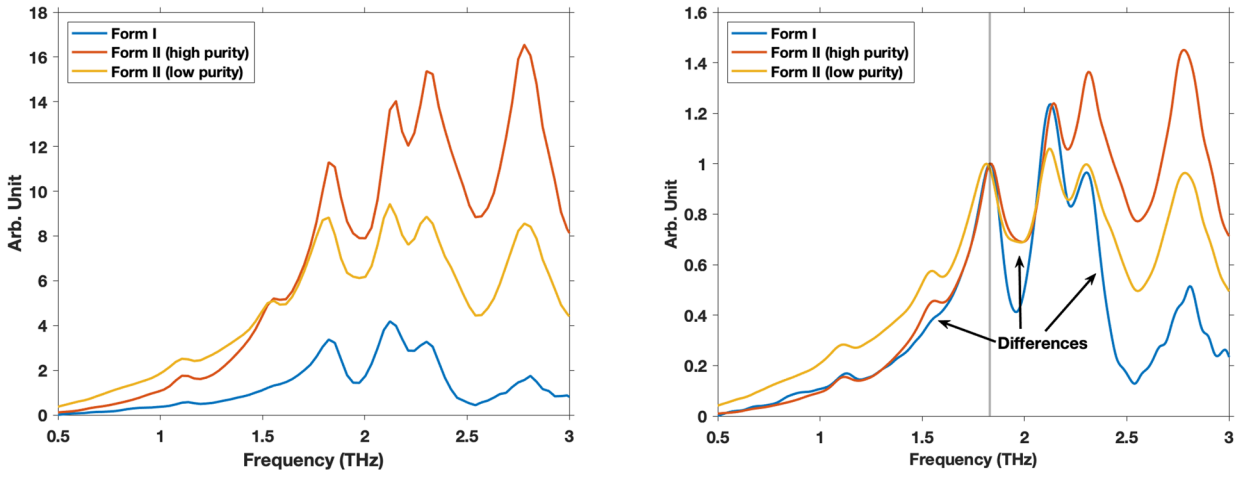

Figure 3. Experimental spectra (left) of aspirin form I (blue), form II with high polymorphic purity (red), and form II with low polymorphic purity (yellow). The spectra (right) are normalized relative to the feature at 1.8 THz (highlighted by the gray vertical line). The arrows highlight the three main noticeable differences between the two forms.

https://doi.org/10.1021/acs.molpharmaceut.1c00727
Mol. Pharmaceutics 2022, 19, 227−234

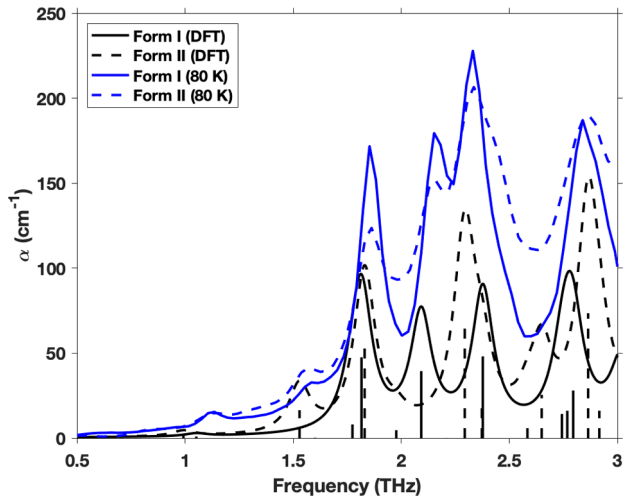

Figure 4. Simulated (black or gray) and experimental (blue) spectra of aspirin form I (solid) and form II (dashed). The vertical bars represent the precise frequencies and intensities for active modes that were predicted by the DFT method for each form. A bandwidth of 1 cm^{-1} was used for the simulated spectra in each case.

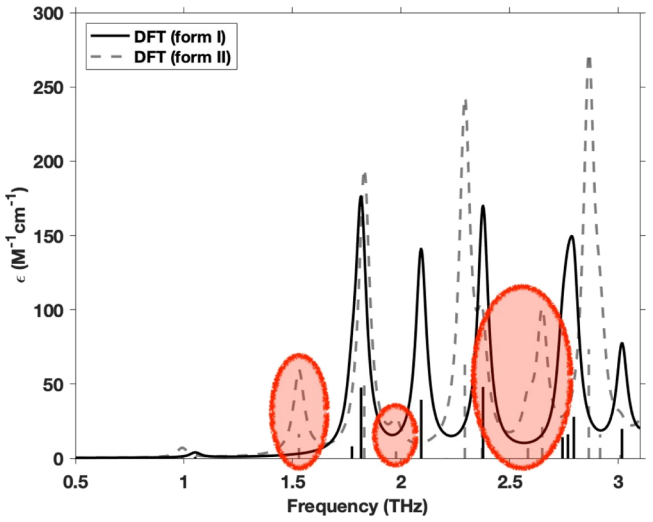

Figure 5. Simulated spectra of forms I and II when the bandwidth was set to 1 cm^{-1}. The red circles highlight the three simulated features predicted in form II that were assigned to the differences in the experimental spectra of form II from form I.

normalize the experimental spectra relative to that feature in Figure 3. The three circled areas correspond to the differences identified between the experimental spectra: (i) The feature at 1.53 THz is predicted only for form II, which explains why the peak is more pronounced in the spectra of the form II samples; (ii) the merging of the peaks just below 2.0 THz in form II can be explained by the extra feature predicted on the high-frequency side of the intense peak at 1.82 THz; (iii) the broad shoulder at 2.5 THz in the experimental spectra of the form II samples matches well with the two less intense peaks at 2.37 and 2.58 THz predicted for form II. Overall, the simulated spectra show a greater degree of difference between the two polymorphs compared to that observed in the experimental spectra. One way to explain this could be the expectation that the form II samples are intergrown with form I domains. To explore this possibility further, a small amount of the "high purity" form II sample was used to spike the bulk form I sample and vice versa. This resulted in an even closer similarity between the experimental spectra. As a final observation, the anticipated structural disorder in the form II samples would be expected to result in noncoherent and less pronounced vibrational motions, which are suggested by the increasing of the baseline in the THz spectra.[33]

To quantify the comparison, the experimental spectra were fitted in Matlab with the spectral features constrained to the frequencies predicted by the simulations, where the peaks were fitted to Lorentzian functions and the baseline was fitted to a power law (eq 1).

$$y = \sum_n \frac{A_n}{\left(1 + \left(\frac{x - f_{c_n - d}}{g_n}\right)^2\right)} + Bx^a + c \quad (1)$$

where A_n is the amplitude of the peak, g_n is the peak width, f_{c_n} is the predicted frequency of the peak, d is the relative shift between the simulated active modes, and $Bx^a + c$ was used to fit the baseline. Application of the shift d is common practice and is mainly due to the difference in temperature between the experimental (80 K) and simulated (0 K) results as well as additional effects of anharmonicity. The fits are shown in Figure 6, and the resulting parameters are shown in Table 2. The highlighted features in both samples are not predicted in the corresponding form but rather in the other polymorph. The fact that it is possible to fit the experimental spectra very closely using this methodology, but that both spectra contain residual features indicative of the other polymorphic form, substantiates the hypothesis that the two polymorphs are intergrown in the samples analyzed and furthermore demonstrates that this feature can be detected by the THz measurements. It is also notable that the baseline fitting parameters of form II in Table 2 are larger than those required for form I, consistent with the expectation that the form II sample is more disordered. This can also be reflected from the wider peak width in form II on average as peak broadening is a significant effect to the THz absorption spectra caused by disorder in crystalline materials.[34,35]

It is evident in Figure 6 that the first peak of form II at 1.0 THz is not fitted as well as the other features. Therefore, further calculations were performed to examine the energies of the structures with the atoms displaced in steps along the eigenvectors corresponding to the first spectral features of each form. Figure 7 shows that the difference between the energy calculated with the harmonic approximation and the real total energy of form II was much larger than that of form I. This implies that the influence of anharmonicity is much larger for the first peak of form II than for form I, which can account for the less effective fitting that is observed. In addition, it was found that the methyl groups ($-CH_3$) in form II were much more active than in form I within the whole low-frequency range (0.5 to 3 THz), showing both rotation around the C$-CH_3$ bond and greater motion of the entire acetyl group. This can be related to differences in the local environments of the CH_3 groups, which include C$-$H$\cdots$O and C$-$H$\cdots\pi$ intermolecular contacts (Figure 8). Two out of three such contacts (within the layers common to the polytypes) are directly comparable in the two polymorphs, but the "interlayer" C$-$H$\cdots$O contact in form I is shorter and closer to linear than that in form II. Hence, the CH_3 groups in form I adopt an approximately symmetrical position between two neighbouring O atoms in form I compared to an asymmetrical arrangement

https://doi.org/10.1021/acs.molpharmaceut.1c00727
Mol. Pharmaceutics 2022, 19, 227−234

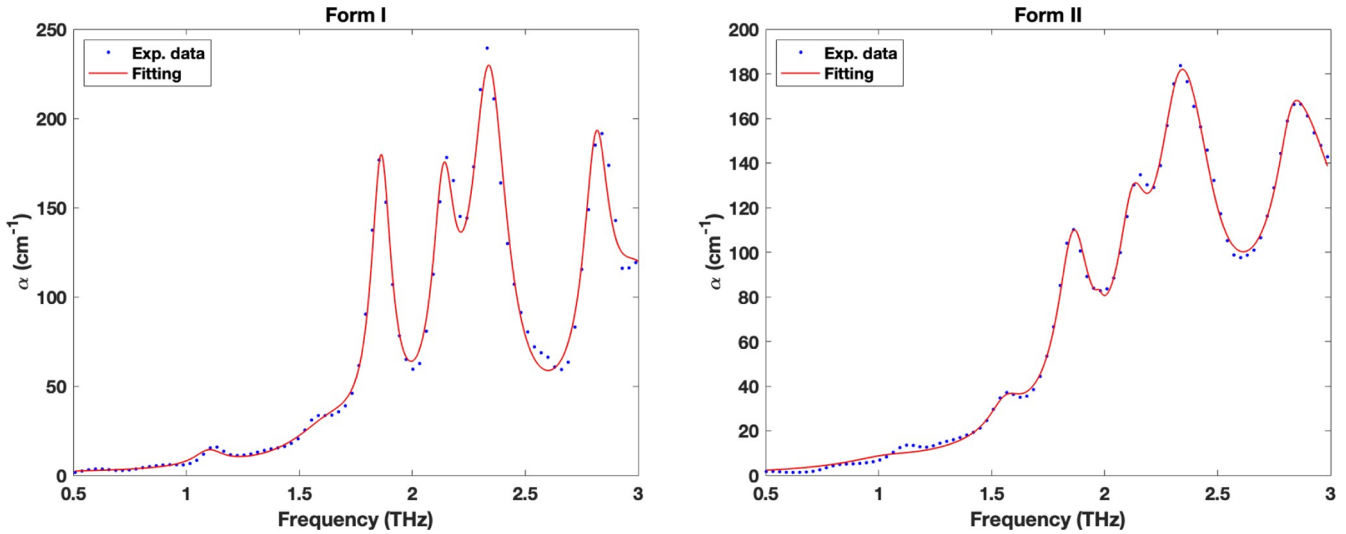

Figure 6. Aspirin form I (left) and form II (right) experimental spectra fitted with the Lorentzian functions and the power law with fixed simulated modes. The blue dots represent the raw data from the experimental data points, while the red curves result from the fitting process.

Table 2. Fitting Parameters for Aspirin Form I and Form II (Top)[a]

	B	a	c	d (THz)	d (cm^{-1})	R^2
form I	0.0164	0.364	0.00285	0.0476	1.59	0.991
form II	1.04	4.14	0.150	0.0329	1.10	0.999
fc$_n$ (THz)			A_n (cm^{-1})		g_n	
1.05			8.82		0.0772	
1.53*			18.2		0.164	
1.81			157		0.0564	
2.10			123		0.0600	
2.29			206		0.0959	
2.38			0.285		0.274	
2.77			134		0.0675	
3.02			99.5		0.198	
fc$_n$ (THz)			A_n (cm^{-1})		g_n	
1.00			3.67		0.209	
1.53			14.5		0.115	
1.83			75.9		0.0876	
1.98			3.58		0.0823	
2.09*			60.3		0.118	
2.29			91.5		0.0848	
2.37			50.0		0.128	
2.79*			45.4		0.538	
2.86			40.3		0.134	

[a]Power law fitting parameters (top). The Lorentzian fitting parameters of form I (middle) and form II (bottom). Features highlighted with an asterisk are not predicted in the corresponding form but rather in the other polymorph.

in form II. The results confirm the observations reported in the early work of Reilly and Tkatchenko.[11]

3.5. Free Energies of the Polymorphs. In Section 3.3 (Table 1), it was shown that the total lattice energy of form I is calculated to be marginally lower than that of form II at absolute zero. To further investigate the relative stability of the polymorphs at real temperatures, the Gibbs free-energy curves of both forms were calculated from 7 to 300 K (shown in Figure S4 and the lower bound being limited by the CRYSTAL17 software package[30]). A turning point is predicted at 75 K, where the Gibbs free energy of form I becomes larger

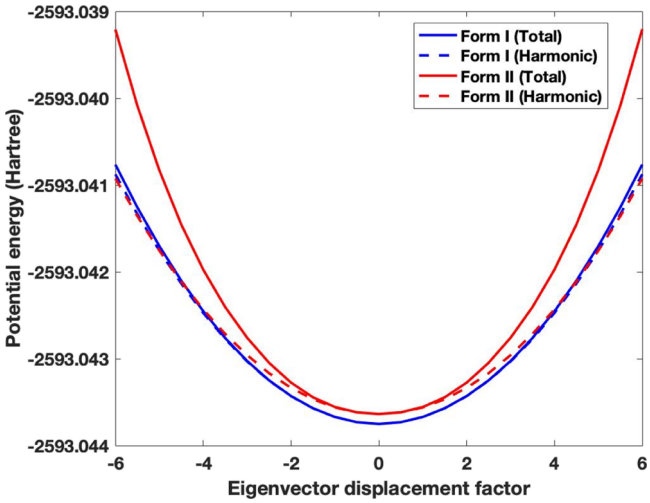

Figure 7. Calculated energies of the structures with the atoms displaced in steps along the eigenvectors corresponding to the first spectral features of form I (blue) and form II (red). The solid lines represent the total energies of the geometry at each position, and the dashed ones are for the energies calculated based on harmonic approximation.

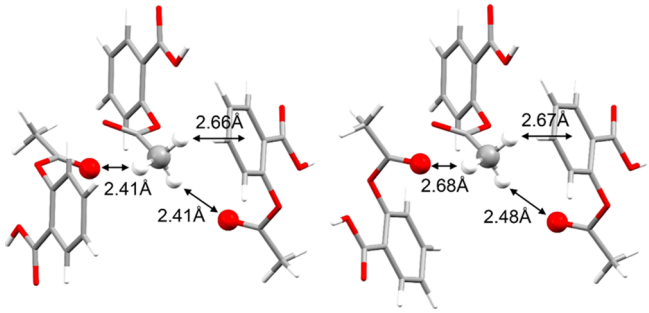

Figure 8. C−H···O and C−H···π intermolecular contacts within the optimized crystal structures of form I (left) and form II (right). The central and right-hand molecules in each diagram lie within the consistent 2D layers of the polytypes, while a different C−H···O contact is formed between layers.

https://doi.org/10.1021/acs.molpharmaceut.1c00727
Mol. Pharmaceutics 2022, 19, 227−234

than that of form II, which infers that form II is more stable at ambient temperature. The dynamic calculations show specifically that the stability of form II arises as a result of its greater vibrational entropy. However, two caveats apply: (1) the free-energy calculation is based on the harmonic approximation, which would be expected to influence the predicted value of the transition point; (2) the calculations refer to the idealized form I and form II crystal structures and do not consider the structural disorder associated with the intergrown nature of form I/form II single crystals.

4. CONCLUSIONS

This work applies THz-TDS and ab initio simulations to explore the two highly similar polymorphs of aspirin. The results show that, even for these two nearly identical crystal structures, THz-TDS can reveal spectral differences based on its sensitivity to inter- and intramolecular forces. With the help of DFT simulations, slight differences observed for the aspirin polymorphs and the spectra provide further solid evidence of the intergrown nature of the two forms. A number of calculated physical properties are compared for the two forms, and most of them are found to be quite similar, reflecting the high degree of structural similarity. However, form II shows a relatively larger vibrational entropy, which yields a lower free energy than form I at temperatures above 75 K. Larger parameters for the baseline fitting of the THz-TDS spectra also indicate a higher degree of structural disorder for form II, consistent with established expectations for this polymorph. The methodology introduced here for aspirin complements existing physicochemical techniques and adds a new perspective to rationalize the crystallography of polymorphic systems and their structural and thermodynamics analyses. Further computational work on a supercell structure incorporating defects would be very valuable to investigate the influence of structural imperfections in the system and could also add insight into possible phase transitions between the aspirin polymorphs. However, a highly efficient computational plan will be required as well as a large amount of computational resource to pursue this work further.

■ ASSOCIATED CONTENT

Supporting Information

The Supporting Information is available free of charge at https://pubs.acs.org/doi/10.1021/acs.molpharmaceut.1c00727.

Spectrum of aspirin form I acquired by Laman et al., XRPD patterns for all samples, additional THz spectra, Gibbs free-energy plot of the two polymorphic forms, crystallographic data for the experimental and simulated crystal structures, and solid-state DFT calculated IR active mode frequencies, symmetry, and intensity (PDF)

Optimized structure of aspirin form I (CIF)

Optimized structure of aspirin form II (CIF)

■ AUTHOR INFORMATION

Corresponding Author

J. Axel Zeitler − *Department of Chemical Engineering and Biotechnology, University of Cambridge, Cambridge CB3 0AS, U.K.*; orcid.org/0000-0002-4958-0582; Phone: +44 (0)1223 334783; Email: jaz22@cam.ac.uk

Authors

Qi Li − *Department of Chemical Engineering and Biotechnology, University of Cambridge, Cambridge CB3 0AS, U.K.*

Andrew D. Bond − *Yusuf Hamied Department of Chemistry, University of Cambridge, Cambridge CB2 1EW, U.K.*; orcid.org/0000-0002-1744-0489

Timothy M. Korter − *Department of Chemistry, Syracuse University, Syracuse, New York 13244, United States*; orcid.org/0000-0002-0398-5680

Complete contact information is available at: https://pubs.acs.org/10.1021/acs.molpharmaceut.1c00727

Notes

The authors declare no competing financial interest.

■ ACKNOWLEDGMENTS

Q.L. would like to thank the Chinese Scholarship Council (CSC) for supporting her Ph.D. study. The computational work was supported via our membership of the UK's HEC Materials Chemistry Consortium, which is funded by EPSRC (EP/L000202, EP/R029431, and EP/T022213), and this work used the ARCHER UK National Supercomputing Service. This work has been performed using resources provided by the Cambridge Tier-2 system operated by the University of Cambridge Research Computing Service (https://www.hpc.cam.ac.uk) funded by EPSRC Tier-2 capital grant EP/P020259/1.

■ REFERENCES

(1) Wheatley, P. J. 1163. The Crystal and Molecular Structure of Aspirin. *J. Chem. Soc.* **1964**, 6036.

(2) Vishweshwar, P.; McMahon, J. A.; Oliveira, M.; Peterson, M. L.; Zaworotko, M. J. The Predictably Elusive Form II of Aspirin. *J. Am. Chem. Soc.* **2005**, *127*, 16802−16803.

(3) Ouvrard, C.; Price, S. L. Toward Crystal Structure Prediction for Conformationally Flexible Molecules: The Headaches Illustrated by Aspirin. *Cryst. Growth Des.* **2004**, *4*, 1119−1127.

(4) Bond, A. D.; Boese, R.; Desiraju, G. R. On the Polymorphism of Aspirin. *Angew. Chem., Int. Ed.* **2007**, *46*, 615−617.

(5) Bond, A. D.; Boese, R.; Desiraju, G. R. On the Polymorphism of Aspirin: Crystalline Aspirin as Intergrowths of Two "Polymorphic" Domains. *Angew. Chem., Int. Ed.* **2007**, *46*, 618−622.

(6) Bond, A. D.; Solanko, K. A.; Parsons, S.; Redder, S.; Boese, R. Single Crystals of Aspirin Form II: Crystallisation and Stability. *CrystEngComm* **2011**, *13*, 399−401.

(7) Crowell, E. L.; Dreger, Z. A.; Gupta, Y. M. High-Pressure Polymorphism of Acetylsalicylic Acid (Aspirin): Raman Spectroscopy. *J. Mol. Struct.* **2015**, *1082*, 29−37.

(8) Shtukenberg, A. G.; Hu, C. T.; Zhu, Q.; Schmidt, M. U.; Xu, W.; Tan, M.; Kahr, B. The Third Ambient Aspirin Polymorph. *Cryst. Growth Des.* **2017**, *17*, 3562−3566.

(9) Polytypism—Online Dictionary of Crystallography https://dictionary.iucr.org/Polytypism (accessed Aug07 2021).

(10) Wen, S.; Beran, G. J. O. Accidental Degeneracy in Crystalline Aspirin: New Insights from High-Level Ab Initio Calculations. *Cryst. Growth Des.* **2012**, *12*, 2169−2172.

(11) Reilly, A. M.; Tkatchenko, A. Role of Dispersion Interactions in the Polymorphism and Entropic Stabilization of the Aspirin Crystal. *Phys. Rev. Lett.* **2014**, *113*, 055701.

(12) Vaksler, Y.; Idrissi, A.; Urzhuntseva, V. v.; Shishkina, S. v. Quantum Chemical Modeling of Mechanical Properties of Aspirin Polymorphic Modifications. *Cryst. Growth Des.* **2021**, *21*, 2176−2186.

(13) Turner, M. J.; Thomas, S. P.; Shi, M. W.; Jayatilaka, D.; Spackman, M. A. Energy Frameworks: Insights into Interaction

Anisotropy and the Mechanical Properties of Molecular Crystals. *Chem. Commun.* **2015**, *51*, 3735−3738.
(14) Chan, E. J.; Welberry, T. R.; Heerdegen, A. P.; Goossens, D. J. Diffuse Scattering Study of Aspirin Forms (I) and (II). *Acta Crystallogr., Sect. B: Struct. Sci.* **2010**, *66*, 696−707.
(15) Chieng, N.; Rades, T.; Aaltonen, J. An Overview of Recent Studies on the Analysis of Pharmaceutical Polymorphs. *J. Pharm. Biomed. Anal.* **2011**, *55*, 618−644.
(16) King, M. D.; Buchanan, W. D.; Korter, T. M. Identification and Quantification of Polymorphism in the Pharmaceutical Compound Diclofenac Acid by Terahertz Spectroscopy and Solid-State Density Functional Theory. *Anal. Chem.* **2011**, *83*, 3786−3792.
(17) King, M. D.; Buchanan, W. D.; Korter, T. M. Understanding the Terahertz Spectra of Crystalline Pharmaceuticals: Terahertz Spectroscopy and Solid-State Density Functional Theory Study of (S)-(+)-Ibuprofen and (RS)-Ibuprofen. *J. Pharm. Sci.* **2011**, *100*, 1116−1129.
(18) Zeitler, J. A.; Newnham, D. A.; Taday, P. F.; Threlfall, T. L.; Lancaster, R. W.; Berg, R. W.; Strachan, C. J.; Pepper, M.; Gordon, K. C.; Rades, T. Characterization of Temperature-Induced Phase Transitions in Five Polymorphic Forms of Sulfathiazole by Terahertz Pulsed Spectroscopy and Differential Scanning Calorimetry. *J. Pharm. Sci.* **2006**, *95*, 2486−2498.
(19) Ruggiero, M. T.; Sibik, J.; Zeitler, J. A.; Korter, T. M. Examination of l-Glutamic Acid Polymorphs by Solid-State Density Functional Theory and Terahertz Spectroscopy. *J. Phys. Chem. A* **2016**, *120*, 7490−7495.
(20) Laman, N.; Harsha, S. S.; Grischkowsky, D. Narrow-Line Waveguide Terahertz Time-Domain Spectroscopy of Aspirin and Aspirin Precursors. *Appl. Spectrosc.* **2008**, *62*, 319−326.
(21) Dovesi, R.; Erba, A.; Orlando, R.; Zicovich-Wilson, C. M.; Civalleri, B.; Maschio, L.; Rérat, M.; Casassa, S.; Baima, J.; Salustro, S.; Kirtman, B. Quantum-mechanical Condensed Matter Simulations with CRYSTAL. *Wiley Interdiscip. Rev.: Comput. Mol. Sci.* **2018**, *8*, No. e1360.
(22) Groom, C. R.; Bruno, I. J.; Lightfoot, M. P.; Ward, S. C. The Cambridge Structural Database. *Acta Crystallogr., Sect. B: Struct. Sci., Cryst. Eng. Mater.* **2016**, *72*, 171−179.
(23) Wilson, C. C. Interesting Proton Behaviour in Molecular Structures. Variable Temperature Neutron Diffraction and Ab Initio Study of Acetylsalicylic Acid: Characterising Librational Motions and Comparing Protons in Different Hydrogen Bonding Potentials . See http://www.rsc.org/suppdata/nj/b2/b203775k/. *New J. Chem.* **2002**, *26*, 1733−1739. Http://Www.Rsc.Org/Suppdata/Nj/B2/B203775k/
(24) Schäfer, A.; Horn, H.; Ahlrichs, R. Fully Optimized Contracted Gaussian Basis Sets for Atoms Li to Kr. *J. Chem. Phys.* **1992**, *97*, 2571−2577.
(25) Perdew, J. P.; Burke, K.; Ernzerhof, M. Generalized Gradient Approximation Made Simple. *Phys. Rev. Lett.* **1996**, *77*, 3865−3868.
(26) Grimme, S.; Antony, J.; Ehrlich, S.; Krieg, H. A Consistent and Accurate *Ab Initio* Parametrization of Density Functional Dispersion Correction (DFT-D) for the 94 Elements H-Pu. *J. Chem. Phys.* **2010**, *132*, 154104.
(27) Grimme, S.; Ehrlich, S.; Goerigk, L. Effect of the Damping Function in Dispersion Corrected Density Functional Theory. *J. Comput. Chem.* **2011**, *32*, 1456−1465.
(28) Donà, L.; Brandenburg, J. G.; Bush, I. J.; Civalleri, B. Cost-Effective Composite Methods for Large-Scale Solid-State Calculations. *Faraday Discuss.* **2020**, *224*, 292−308.
(29) Noel, Y.; Zicovich-Wilson, C. M.; Civalleri, B.; D'Arco, Ph.; Dovesi, R. Polarization Properties of ZnO and BeO:AnAb Initio Study through the Berry Phase and Wannier Functions Approaches. *Phys. Rev. B: Condens. Matter Mater. Phys.* **2001**, *65*, 014111.
(30) Pascale, F.; Zicovich-Wilson, C. M.; López Gejo, F.; Civalleri, B.; Orlando, R.; Dovesi, R. The Calculation of the Vibrational Frequencies of Crystalline Compounds and Its Implementation in the CRYSTAL Code. *J. Comput. Chem.* **2004**, *25*, 888−897.
(31) Boys, S. F.; Bernardi, F. The Calculation of Small Molecular Interactions by the Differences of Separate Total Energies. Some Procedures with Reduced Errors. *Mol. Phys.* **2002**, *100*, 65−73.
(32) Jepsen, P. U.; Fischer, B. M. Dynamic Range in Terahertz Time-Domain Transmission and Reflection Spectroscopy. *Opt. Lett.* **2005**, *30*, 29.
(33) Sibik, J.; Zeitler, J. A. Direct Measurement of Molecular Mobility and Crystallisation of Amorphous Pharmaceuticals Using Terahertz Spectroscopy. *Adv. Drug Delivery Rev.* **2016**, *100*, 147−157.
(34) Tan, N. Y.; Zeitler, J. A. Probing Phase Transitions in Simvastatin with Terahertz Time-Domain Spectroscopy. *Mol. Pharm.* **2015**, *12*, 810−815.
(35) Nickel, D. V.; Ruggiero, M. T.; Korter, T. M.; Mittleman, D. M. Terahertz Disorder-Localized Rotational Modes and Lattice Vibrational Modes in the Orientationally-Disordered and Ordered Phases of Camphor. *Phys. Chem. Chem. Phys.* **2015**, *17*, 6734−6740.

https://doi.org/10.1021/acs.molpharmaceut.1c00727
Mol. Pharmaceutics 2022, 19, 227−234